RSC Advances

PAPER

View Article Online
View Journal | View Issue

Cite this: *RSC Adv.*, 2019, **9**, 32535

Sandwiching analytes with structurally diverse plasmonic nanoparticles on paper substrates for surface enhanced Raman spectroscopy†

Jemima A. Lartey, John P. Harms, Richard Frimpong, Christopher C. Mulligan,* Jeremy D. Driskell* and Jun-Hyun Kim*

This report describes the systematic combination of structurally diverse plasmonic metal nanoparticles (AgNPs, AuNPs, Ag core–Au shell NPs, and anisotropic AuNPs) on flexible paper-based materials to induce signal-enhancing environments for surface enhanced Raman spectroscopy (SERS) applications. The anisotropic AuNP-modified paper exhibits the highest SERS response due to the surface area and the nature of the broad surface plasmon resonance (SPR) neighboring the Raman excitation wavelength. The subsequent addition of a second layer with these four NPs (*e.g.*, sandwich arrangement) leads to the notable increase of the SERS signals by inducing a high probability of electromagnetic field environments associated with the interparticle SPR coupling and hot spots. After examining sixteen total combinations, the highest SERS response is obtained from the second layer with AgNPs on the anisotropic AuNP paper substrate, which allows for a higher calibration sensitivity and wider dynamic range than those of typical AuNP–AuNP arrangement. The variation of the SERS signals is also found to be below 20% based on multiple measurements (both intra-sample and inter-sample). Furthermore, the degree of SERS signal reductions for the sandwiched analytes is notably slow, indicating their increased long-term stability. The optimized combination is then employed in the detection of let-7f microRNA to demonstrate their practicability as SERS substrates. Precisely introducing interparticle coupling and hot spots with readily available plasmonic NPs still allows for the design of inexpensive and practical signal enhancing substrates that are capable of increasing the calibration sensitivity, extending the dynamic range, and lowering the detection limit of various organic and biological molecules.

Received 14th July 2019
Accepted 4th October 2019

DOI: 10.1039/c9ra05399a

rsc.li/rsc-advances

Introduction

Surface enhanced Raman scattering (SERS) spectroscopy is a powerful analytical tool that has received much attention because of its simplicity, high sensitivity and selectivity.[1–4] SERS involves a Raman scattering signal associated with small energy changes of the light scattered from a vibrating molecule adsorbed on a metallic surface. The use of plasmonic metal nanostructures has readily improved these vibrational signals by providing both chemical and electromagnetic enhancements.[2,5–8] Although the SERS enhancement mechanisms are complicated, the electromagnetic enhancement (EM) effect is thought to explain the strongest contribution of the molecular vibration at the surface of metal particles by plasmon resonance excitation. Further signal enhancement can be achieved by properly controlling the interparticle coupling environments and multiple junctions between nanoscale structures (*i.e.*, hot spots), where extraordinarily strong local electric fields are often generated near the vicinity of nanoscale materials possessing surface plasmon resonance (SPR).[2,6,9,10]

The signal enhancements by SERS have been highly tuned by the characteristics of the substrates associated with the plasmonic properties and morphology of the nanostructures.[1,3,8,11,12] As such, enormous efforts have been made to the development of structurally diverse plasmonic materials and new fabrication strategies capable of finely tuning their arrangements for SERS enhancement. These approaches readily improve the SERS sensitivity, but often require complicated multiple steps to control morphological features, significantly limiting their practical use as rapid and inexpensive SERS substrates. However, little attention has been paid to the further improvement of currently-available, simple systems and/or easy modification strategies using conventional plasmonic nanomaterials to generate the proper environment for SERS enhancement, where the probability of SPR coupling and hot spots could be maximized.

The critical requirements for designing practical SERS substrates for routine analytical measurements include cost-effectiveness, high sensitivity, reproducibility, and long-term

Department of Chemistry, Illinois State University, Normal, Illinois 61790-4160, USA. E-mail: cmullig@ilstu.edu; jdriske@ilstu.edu; jkim5@ilstu.edu

† Electronic supplementary information (ESI) available. See DOI: 10.1039/c9ra05399a

stability. The immobilization of plasmonic nanoparticles (NPs) onto flexible solid surfaces has shown the possibility to fulfil these requirements.[13–20] The use of paper-based materials could potentially bring interesting features, including high flexibility, biocompatibility, and biodegradability, while providing minimal background interference upon the incorporation of plasmonic metal NPs. In addition, properly modifying paper with plasmonic NPs can readily reduce uncertain fluorescence in the visible wavelength area (*e.g.*, ~440 nm) during SERS measurements,[14,21] which may be an extra benefit of utilizing inexpensive paper-based materials as SERS substrate.

Current efforts to develop paper-based SERS substrates have established proof of principle and address many fabrication needs. However, the inability to control the nanostructure architecture limits the overall enhancement factors achieved with these paper-based substrates. Numerous studies have established that molecules located in the gap between closely spaced NPs experience the greatest SERS enhancement. Thus, an ideal SERS substrate would incorporate the attributes of a paper-based substrate and capitalize on the enhancement generated by precise control of NP spacing to generate hot spots. In this work, we explore the direct application of an additional layer of metal nanostructures onto plasmonic paper substrates to induce a new environment where the SPR and interparticle coupling can further improve SERS responses. This approach is attractive since it simplifies the entire fabrication strategy in a controlled manner with readily available plasmonic particles on filter paper.

Here we compared SERS responses using four types of conventional metal NPs (*e.g.*, AgNPs, AuNPs, Ag core–Au shell NPs, and anisotropic AuNPs) after loading them onto filter paper. Another layer of these NPs was then applied to each of the different plasmonic papers to form a sandwich-like structure, which introduced a stronger EM field environment across the filter paper for SERS measurements (Fig. S1†).[2,10,20,22] This sandwich geometry creates additional local aggregates to induce a high probability of having sensing molecules reside between the NP gaps and junctions (*i.e.*, NP-analyte-NP arrangement), thereby notably improving the SERS sensitivity. Thus, we thoroughly examined the degree of the SERS enhancements of the initial and sandwiched analytes on plasmonic papers to understand not only the amplified EM effect associated with abundant interparticle SPR coupling and hot spots, but also the structural impact on long-term stability, reproducibility, and applicability in biological systems. Based on 16 combinations using the four different NPs, the sandwich arrangement from the first layer with anisotropic Au and the second layer with AgNPs responded to give the highest SERS signals, which were presumably due to the large surface areas and enhanced EM effect. This improved system was employed in SERS-based biological molecule detection (let-7f microRNA), which was compared to the sandwich structures using typical AuNPs. Our study readily allows for understanding the capability of further improving SERS upon precisely modifying a fabrication strategy even with conventional NPs. The high simplicity and applicability of sandwiching analytes with structurally diverse plasmonic NPs on paper-based materials supports the development of inexpensive and practical signal enhancing systems equipped with minimal background noise and a low detection limit for various molecules.

Experimental

Materials and methods

Hydrochloric acid, nitric acid, trisodium citrate, potassium hydroxide, isopropyl alcohol, hydrogen tetrachloroaurate(III) trihydrate ($HAuCl_4 \cdot 3H_2O$), sodium borohydride ($NaBH_4$), potassium carbonate (K_2CO_3), L-ascorbic acid sodium salt (AsA), hexadecyltrimethylammonium bromide (CTAB, ≥99.0%), silver nitrate ($AgNO_3$), 4-nitrobenzenethiol (4-NBT), and Whatman filter paper (grade 40) were purchased from Fisher Scientific; all of the chemicals were used without purification. microRNA, let-7f, was purchased from Integrated DNA Technologies (IDT), and resuspended in RNase- and DNase-free water to a final concentration of 100 μM. The pure water was obtained from the Nanopure Water System (Barnstead/Thermolyne).

Synthetic procedures for the four different types of plasmonic nanoparticles

AuNPs and AgNPs with ~60 nm diameters were prepared by the modified thermal reduction method.[23–26] An aliquot (2.0 mL) of gold (1 wt% $HAuCl_4 \cdot 3H_2O$) or silver (0.5 wt% $AgNO_3$) solution was diluted in 100 mL of water in a 250 mL Erlenmeyer flask containing a magnetic stirring bar. After vigorously stirring the solution for 15 min, the flask was heated to boiling. 1 wt% trisodium citrate (1.5 mL for gold and 4.0 mL for silver) was quickly added to the boiling solution, which led to the formation of spherical AuNPs or AgNPs. After completing the reaction, the final solution was adjusted to ~80 mL in total volume (exhibiting an extinction maximum of ~2.4) and stored at room temperature without further purification prior to use.

Ag core–Au shell NPs were prepared by our *in situ* method.[27] Initially, K_2CO_3 (0.025 g) was fully dissolved in 100 mL water in a 150 mL Erlenmeyer flask. A 1 wt% $HAuCl_4 \cdot H_2O$ solution (2.0 mL) was then added to this solution, whose solution color changed from light yellow to colorless within 30 min (K-gold solution). Similarly, 0.5 wt% $AgNO_3$ was prepared in an aqueous solution of K_2CO_3, which exhibited a color change from colorless to bright yellow in a few seconds (K-silver solution). These two solutions were stored in a refrigerator overnight prior to use. An aliquot (10 mL) of the aged silver solution was placed in a 24 mL glass vial containing a magnetic stirring bar. The sequential addition of AsA (0.6 mL of 100 mM) and the aged gold solution (6.0 mL) to the silver solution led to the gradual color changes from yellow, green, and brownish-blue in 5 min. The final solution was centrifuged at 3000 rpm for 20 min (Sorvall Legend X1 Centrifuge Series) and the precipitates were re-suspended in ~10 mL water to exhibit an extinction peak of ~2.4.

A seed-growth method was used to prepare the anisotropic AuNPs.[28] The aged K-silver solution (10 mL) was placed in a 24 mL glass vial containing a magnetic stirring bar. The sequential addition of $NaBH_4$ (0.04 mL of 3.2 mM) and AsA

(0.6 mL of 100 mM) to the silver solution resulted in the formation of dark yellow Ag seeds. The aged K-gold solution (6.0 mL) was then added dropwise into this mixture, leading to the formation of small seed NPs with a brownish-purple color. After aging the seeds for a few hours, a preheated CTAB solution (10 mL of 10 mM, $\geq$ 35 °C) containing 1 wt% $HAuCl_4 \cdot H_2O$ solution (0.2 mL) and 100 mM of AsA (0.6 mL) was placed in a 15 mL polystyrene centrifuge tube. Shortly afterwards, an aliquot of the seeds (1.75–2.0 mL) was added to the colorless CTAB solution, which was placed under a fluorescent light (a 35 W desk lamp providing ~80 mW cm^{-2}, measured by a handheld optical powder meter; Newport Corp.) for 40 min. The final solution was centrifuged at 3000 rpm for 20 min twice, and the precipitates were re-suspended in water to exhibit an extinction peak of ~2.4 (*e.g.*, typically a 6-fold dilution based on the volume of the seed solution).

Preparation of paper-based plasmonic substrates and their photothermal heating properties under a broadband light source

The four different types of plasmonic NPs prepared above were loaded onto filter papers by a dipping method.[16,20,29,30] Filter papers (Whatman grade no. 40, 55 mm in diameter) that were dried at 50 °C in an oven overnight were immersed in 10 mL of the NP solution in plastic Petri dishes (60 mm × 15 mm). After soaking for 24 h, the filter papers were dried in the oven. The loading efficiency of the NPs onto the filter papers was estimated by monitoring the changes of the extinction of the initial and remaining NP solutions. In addition, the photothermal heating profiles of these filter papers (~1 cm × 1 cm) was examined under a solar-simulated light (providing ~100 mW cm^{-2}, a continuous Xe arc lamp equipped with an optical filter, Newport Inc.). As our previous work demonstrated the linear relationship between the output temperature and the loaded amount of NPs onto filter paper,[29] the photothermal heating of these four different plasmonic papers under comparable NP loading could directly explain their structure- and/or packing-dependent properties. As a comparison, unmodified glass slides (18 mm in diameter, G CVR glass, Fisher Scientific) were treated under the same preparation conditions. In addition, similar amounts of NPs as were loaded onto the filter paper were dropped and dried on the glass slides to examine their photothermal heating and SERS responses.

Surface enhanced Raman spectroscopy (SERS) measurements under various conditions

A series of filter papers loaded with different types of plasmonic NPs were cut into ~1 × 1 cm^2 squares and treated with 2.0 mL of the 4-NBT solution (the concentration ranged from 1 mM to 1 nM of 4-NBT in acetonitrile) in glass vials for 30 min. These filter papers were then rinsed with acetonitrile and allowed to dry prior to the SERS analysis (785 nm laser with ~5.5 mW intensity). A subsequent second layer was formed by applying an aliquot of the metal NP solution (0.5 mL) onto half (0.5 cm × 1.0 cm) of the initial plasmonic paper for 30 min (4 types of paper × 4 types of metal NPs in triplicate). The final papers were then dried prior to the SERS analysis. At least 3 pieces of paper were tested at a minimum of 3 spots per sample. To calculate the SERS enhancement factors (EFs), the most common method utilizing the following equation was used, $EF = (I_{SERS} \times C_{Raman})/(I_{Raman} \times C_{SERS})$.[31,32] I_{Raman} was collected from the bare filter paper (1 × 1 cm^2) soaked in an aliquot of highly concentrated 4-NBT (2.0 mL of 100 mM) in acetonitrile and I_{SERS} was acquired from the plasmonic paper soaked in an aliquot of 1 μM of 4-NBT solution. To demonstrate the applicability of sandwiching analytes with plasmonic NPs for the detection of biological molecules by SERS, an aliquot of let-7f microRNA suspended in HyPure molecular grade water (50 μL of 1 μM) was applied to the filter paper (~1 × 1 cm^2) loaded with spherical and anisotropic AuNPs (3 mm diameter, prepared by a single-hole punch). After 10 min of incubation, the plasmonic paper was dried with a stream of N_2 gas. The second layer was subsequently formed with spherical AuNPs and AgNPs (50 μL) to examine the signal enhancements by SERS. All spectra were averaged after measuring a minimum of ten different spots.

Instrumentation

An environmental scanning electron microscope (SEM, FEI-Quanta 450 instrument at operating at a voltage of 20 kV) was used to analyze the general size distribution and evaluate the overall morphology and compositions of plasmonic NPs on the filter paper. The paper samples were coated with a thin gold film using a Denton vacuum sputter coater (DESK II) to avoid charging problems during image analysis. A transmission electron microscope (TEM, Hitachi H8100 operating at an accelerating voltage of 200 kV) was used to examine the structural properties of the plasmonic NPs after depositing them on a 300-mesh carbon-coated copper grid. A UV-Visible spectrometer (UV-Vis, Agilent) was used over the wavelength range of 200 to 1100 nm to characterize the absorption property of the metal NPs. All plasmonic NPs were suspended in water and transferred to a quartz UV-Vis cell. The amount of NPs loaded onto each filter paper was calculated by using the standard solutions of metal NPs *via* the Beer–Lambert law. A surface UV-Vis-IR spectrophotometer equipped with a reflectance probe (StellarNet) was used to examine the absorption property (300 nm–1700 nm) of the resulting plasmonic paper. A dynamic light scattering and zeta potential instrument (DLS, ZetaPALS, Brookhaven Instruments Corp.) equipped with a 35 mW solid state laser at 90° was used to measure the hydrodynamic diameter and polydispersity as well as the surface charge of the plasmonic metal NPs at 20 °C. All samples were diluted in pure water. The data were collected from an average of five measurements. Real-time temperature profiles of the plasmonic samples were collected by an infrared thermal image analyzer (Fluka FLIR40, Global Test Supply). The intensity of the solar-simulated light source was estimated by a handheld optical power meter (1916 C Power Meter, Newport Inc.). For typical SERS measurements, all samples were scanned for 1 second or 3 seconds using a benchtop ProRaman-L (Enwave Optronics) equipped with a 785 nm laser. The intensity of the

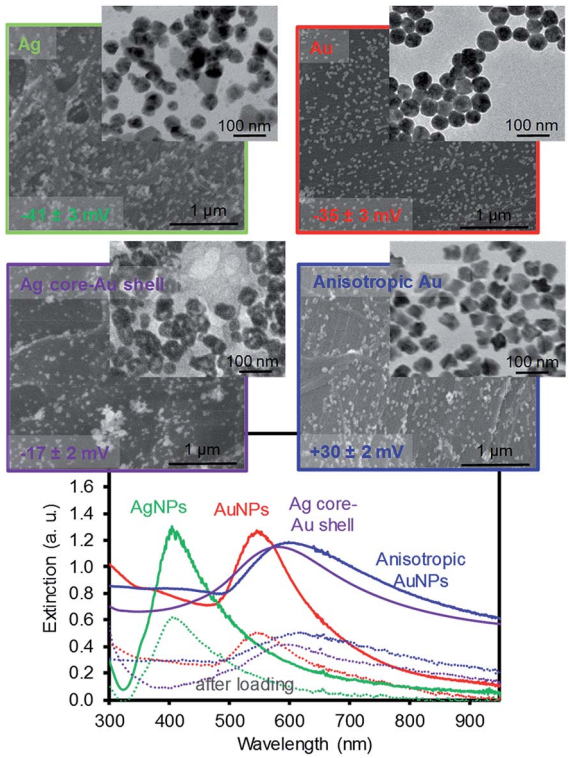

Fig. 1 SEM and TEM images of the four types of plasmonic NPs on filter paper and their corresponding SPR patterns before and after the loading of NPs using a two-fold diluted solution.

laser source was adjusted ~5.5 mW by measuring with the PM100USB power meter (Thor Labs).

Results and discussion

Fig. 1 shows the images of the four types of plasmonic NPs with comparable sizes that were loaded onto filter paper by dip coating. Both the AgNPs and AuNPs were prepared by the thermal reduction method using trisodium citrate, and the AgNPs were slightly less uniform and had a higher tendency to form more aggregates on the filter paper. The Ag core–Au shell NPs exhibited the presence of some cavities near the inner cores (TEM image) due to the contribution of the galvanic reaction during the sequential reduction of the silver and gold ions with AsA.[27] The absence of strong stabilizing agents around these core–shell NPs resulted in the formation of relatively large aggregates on the filter paper. This speculation was supported by the surface charge of these NPs, where the zeta potential measurements showed ≤ -35 mV for both citrate-stabilized AgNPs and AuNPs, $\geq +30$ mV for anisotropic AuNPs, and around -17 mV for Ag core–Au shell NPs. The anisotropic AuNPs were prepared by a seed growth method and showed slightly rough surfaces compared to the rest of the NPs, but were well distributed with local aggregates (*e.g.*, clustering of a few NPs) on the filter paper. The corresponding extinction patterns (*i.e.*, SPR) elucidated the structural features and distribution of these NPs in solution. For example, the AgNPs with the broader SPR band implied a much higher polydispersity than the AuNPs with a narrower SPR band. The Ag core–Au shell NPs exhibited a slightly longer and broader SPR band than that of the spherical AuNPs, which indicated the presence of a phase boundary between the two metals and a slightly higher polydispersity.[27] The anisotropic AuNPs exhibited a relatively broader and longer SPR band than the Ag core–Au shell NPs because of their surface roughness with the wide size distribution. To prepare the plasmonic paper, filter paper that was dried in an oven was soaked in the NP solutions overnight at room temperature. The loading process onto the filter paper was almost identical for all NP solutions with an extinction maximum of ~2.4. However, the loading efficiency of the NPs varied slightly within the extinction of ~0.12, which was estimated by the SPR band reduction before (solid lines) and after (dotted lines) the dip coating (shown in Fig. 1).

Fig. 2 shows the digital photos of the plasmonic paper loaded with these four types of NPs and their corresponding photothermal heating property and absorption pattern. The color of the paper clearly indicated the formation of distinctively different plasmonic papers whose surfaces were uniformly packed with the NPs. The photothermal heating property of these plasmonic papers was then examined under a broadband light source (~100 mW cm^{-2}). Although the heating efficiency of substrates is often affected by the loaded amount of plasmonic NPs,[29,33–35] the temperature profiles of the plasmonic paper (1 × 1 cm^2) loaded with comparable amounts of NPs could explain the structural property and packing pattern of the NPs. The anisotropic AuNPs and AgNPs showed the highest and lowest heating profiles, respectively, as monitored by an IR thermal camera in real time; these light-induced heating patterns were presumably due to the surface areas and absorption properties, as well as the way the NPs were packed onto the filter paper. The higher temperature distribution for the anisotropic AuNPs could have been caused by the increasing Coulomb interaction of the NPs and/or interparticle coupling of SPRs (*e.g.*, accumulative effect) on the paper supported systems.[29,33,36,37] The entire area of the plasmonic paper

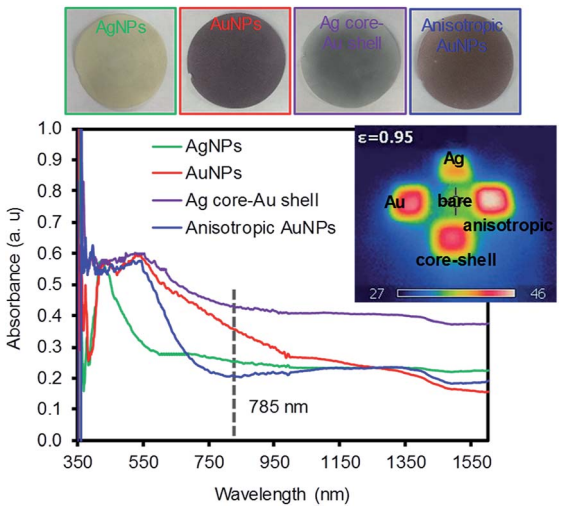

Fig. 2 Digital photos of the four types of plasmonic NPs on filter paper and their corresponding absorption patterns.

displayed moderate heating, but the actual temperatures near the surface of the NPs were expected to be much higher given their photothermal heating capability. This heating behavior (*e.g.*, local heating of the plasmonic paper) could contribute to the sensing capability of SERS-based molecular vibrational spectroscopy.[29,38,39] This is because SERS utilizes a coherent laser source in the near infrared (*e.g.*, 785 nm) that enhances the local electromagnetic (EM) field due to the SPR of plasmonic NPs induces the photothermal heating of the plasmonic substrates, thereby impacting the adsorption configuration and vibration of the sensing molecules. Loading these NPs onto the filter paper readily facilitated local aggregation, which could make these prepared papers suitable as SERS substrates. Unlike well-dispersed plasmonic NPs in solution, the degree of local aggregation and/or plasmonic coupling was also examined by the surface UV-Vis-IR absorption patterns based on the way these plasmonic NPs were packed on the paper substrates. Although obtaining strong absorption patterns from 2-dimensional substrates is difficult due to the nature of reflectance measurement conditions particularly with a strong absorber paper surface,[40,41] the appearance of detectable additional peaks at longer wavelengths with respect to the NPs in solution clearly indicates the presence of local aggregates of plasmonic NPs on the filter paper (Fig. S2†).[42–47] These phenomena have been explained by the formation of small gaps between adjacent particles to induce interparticle plasmonic coupling whose spacing governs the degree of the wavelength shift. Specifically, the silver plasmonic paper displayed one intense peak at 400 nm and a small band at 700 nm where the latter peak might arise from the strongly induced NP interactions in the large areas of randomly aggregated AgNPs.[48] The gold plasmonic paper only showed one peak, which became broader in the entire visible range, probably due to the somewhat uniform formation of local aggregates. The absorbance of the core–shell plasmonic paper almost disappeared due to the severe aggregation of NPs, whereas the anisotropic plasmonic paper with a detectable broad peak over 950 nm implied the presence of plasmonic coupling caused by locally clustered anisotropic NPs along with their inter-cluster coupling. The packing and distribution pattern of the NPs confirmed by the surface absorption patterns were notably different from the NPs in solution and could influence the degree of the SERS enhancements.

These four types of plasmonic filter papers were initially dropped with an aliquot of a Raman reporter (1 mM of 4-NBT) to examine their SERS responses using a 785 nm Raman laser source (Fig. 3). Upon the chemical adsorption of 4-NBT by self-assembly, all these substrates clearly provided intense signals at 1078 cm^{-1} for the C–S vibration, 1106 cm^{-1}/1180 cm^{-1} for the C–H bending and stretching, ~1336 cm^{-1} for the N–O vibration, and 1570 cm^{-1} for the ring C–C stretching.[49–52] Among these peaks, the most intense peak corresponding the N–O vibrational mode of the NO_2 group was compared to another peak where the maximum peak position of NO_2 was slightly shifted depending on the type of plasmonic paper. In addition, the percent relative standard deviation (% RSD) of the SERS signals was below 15% (except the silver plasmonic paper with ~20%),

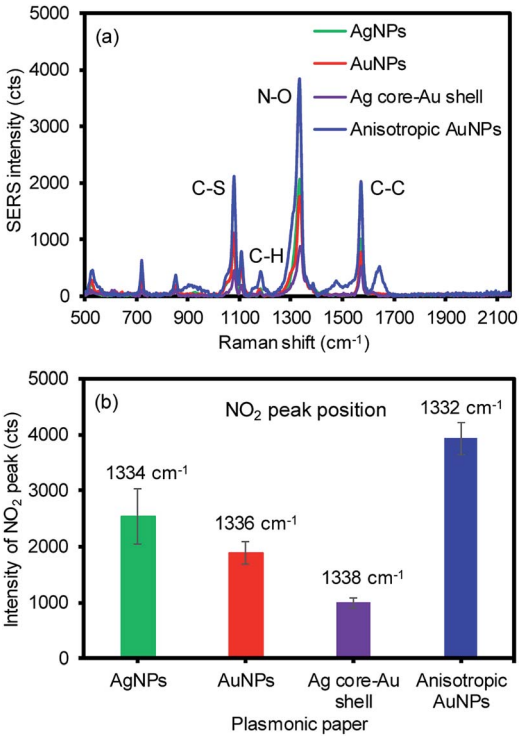

Fig. 3 Representative (a) SERS spectra with four different plasmonic papers and (b) their most intense peak wavenumber (average of minimum 9 spots from 3 plasmonic papers under single scan).

based on several intra-sample (within a sample substrate) and inter-sample (sample-to-sample) measurements. This observation and the way the plasmonic NPs were packed across the filter paper strongly indicated that the entire preparation process of these plasmonic papers was reproducible. The anisotropic AuNPs on the filter paper exhibited the greatest SERS response, which was typically 2–4 times higher than the rest of the plasmonic papers due to the increased surface area, EM effect from the sharper structural features (corners and edges), and the nature of the broad SPR band.

Additional plasmonic NPs were then applied to form a sandwich geometry to introduce the increased probability of placing the analyte between the NPs on the paper substrates, which could additionally create interparticle coupling environments (*e.g.*, a high density of SPR coupling and hot spots) to take full advantage of the EM effect (Fig. 4). As expected, all SERS signals were detectably improved after applying the second layer with these four plasmonic NPs along with the corresponding SERS enhancement factors (EFs) regardless of the types of NPs. Among the 16 combinations of plasmonic NPs, the anisotropic AuNP-loaded paper greatly improved the SERS signals, particularly with the second layer of AgNPs. The first layer of anisotropic AuNPs with the rough surfaces could have allowed for the greater adsorption of analytes to exhibit initially higher SERS signals by the chemical and EM enhancements.[11] Applying the second layer with the AgNPs resulted in much higher enhancements by inducing stronger EM fields due to the high extinction coefficient of silver, compared to the gold-

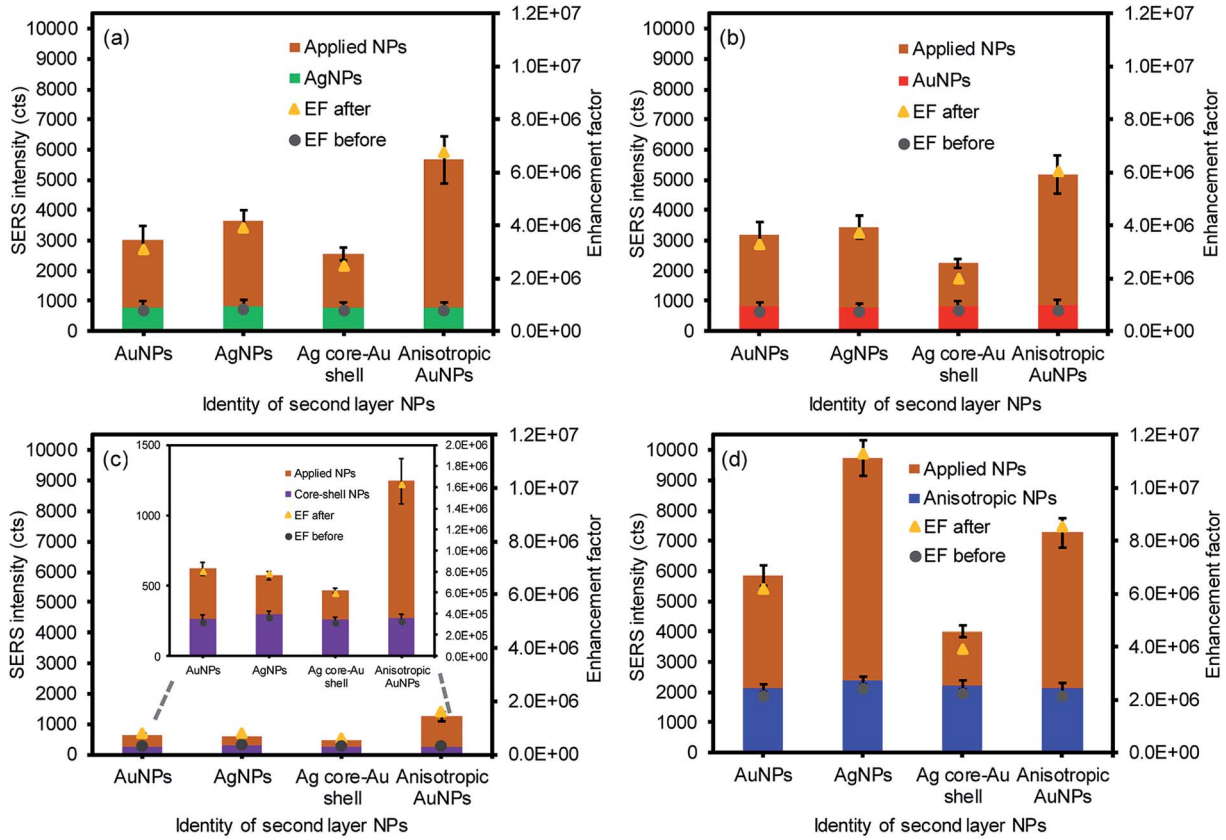

Fig. 4 Average SERS signals and EFs before and after applying four different NPs onto (a) AgNP, (b) AuNP, (c) Ag core–Au shell, and (d) anisotropic AuNP plasmonic paper treated with 1 μM of 4-NBT (average of minimum 9 spots from 3 plasmonic papers).

derived materials.[53–55] Interestingly, the inverse sandwich arrangement (*i.e.*, the first layer of the AgNPs and the second layer of the anisotropic AuNPs) showed a detectably lower SERS response, which might be associated with the slightly poor adsorption of 4-NBT onto the AgNP-loaded paper substrate under the same treatment. The smooth surface of the spherical AgNPs with relatively smaller surface areas could limit the efficient uptake of the analytes. The overall EFs of the sandwiched NPs on the filter paper with the treatment of 1 μM analyte solution were comparable or superior to the results shown in the literature without the need for extensive structural modification or precise arrangement of plasmonic NPs.[13,32,56] Even when we used the readily available plasmonic NPs, the way the plasmonic NPs were treated still allowed for the significant improvement of the SERS signals by introducing rich environments for abundant interparticle coupling and a high density of random hot spot sites.

As the above experiment verified the apparent SERS enhancements from sandwiching the analytes with the plasmonic NPs, the sensing capability of the plasmonic paper loaded with the AuNPs and anisotropic AuNPs was then compared as a function of the 4-NBT concentration (SERS intensities *vs.* logarithm of 4-NBT concentrations shown Fig. 5). The anisotropic AuNP-loaded papers exhibited notably higher signals than those of the spherical AuNPs, regardless of the concentration of 4-NBT (1 nM–1 mM). This pattern clearly explained the importance of the type of plasmonic NPs on the SERS sensitivity, where the linear dynamic range for the anisotropic AuNP paper (~6 orders of magnitude) was relatively

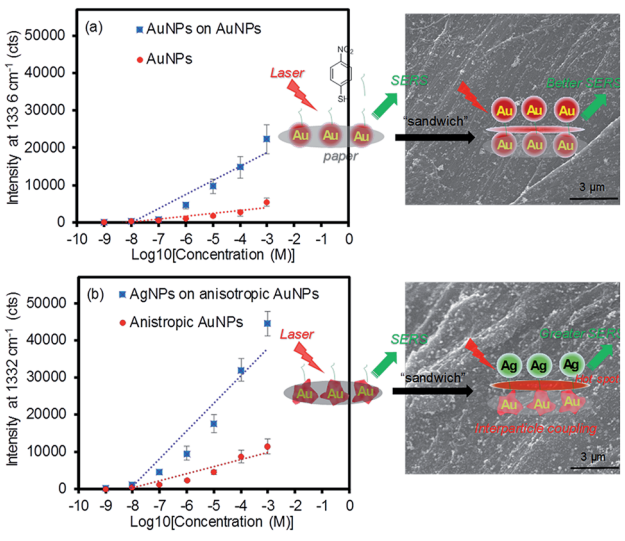

Fig. 5 SERS intensity of 4-NBT as a function of the concentration before and after applying another layer of NPs and their representative SEM images; (a) AuNPs on AuNP plasmonic paper and (b) AgNPs on anisotropic AuNP plasmonic paper.

wider than that of the typical spherical AuNP paper (~4 orders of magnitude) under the same treatments.[16,29,57] To amplify the EM effect,[22,57,58] the second layer of plasmonic NPs resulted in a much higher calibration sensitivity (~2-fold) and a wider dynamic range, particularly for the combination of AgNPs and anisotropic AuNPs. Interestingly, the signal enhancements before and after applying the plasmonic NPs on the filter paper steadily decreased with a decrease in the concentration of 4-NBT. Specifically, the anisotropic AuNP-plasmonic paper treated with the concentrations of the 4-NBT solution between 1 mM and 1 μM led to the improvement of the SERS signals at a minimum of 2–3 times upon the formation of the sandwich layers. However, the same system marginally increased the SERS signals at the 4-NBT concentrations of 10 nM and 1 nM. This disproportional enhancement was possibly due to the presence of fewer molecules by slower/limited adsorption kinetics onto the plasmonic paper at the low concentrations (Fig. S3†), which could also have reduced the EF effect environments after the NPs were sandwiched. Similarly, the limited SERS enhancements from the plasmonic paper loaded with the spherical AuNPs (even after applying another layer of spherical AuNPs) were possibly caused by the low coverage of 4-NBT at low concentrations compared to the anisotropic AuNPs in a given time period. The spherical AuNPs with relatively low surface areas required a long interaction time with 4-NBT to improve their SERS sensitivity. All experimental conditions were identical (except for the concentration of 4-NBT) to minimize the variables in this study. The representative low and high magnification SEM images (prepared after applying another layer of plasmonic NPs) shown in Fig. 5 and S4† clearly display an additional number of NPs and locally aggregated clusters across the paper substrates which positively contributed to the SERS enhancements.

The control experiment, applying the 4-NBT analyte onto the pre-sandwiched layers of AuNPs, resulted in the appreciable reduction of the SERS intensity with a slight rise of the background baseline, particularly at low concentrations of SERS analytes and/or without a baseline correction (Fig. S5†). This trend was often observed when the substrate was treated with relatively low concentrations of the analytes and measured without using a baseline correction function. The substrate might have behaved similarly to the plasmonic paper loaded with excess NPs because the formation of large colloidal aggregates beyond the optimal cluster limit could have blocked the hot spot areas and resulted in detrimental SERS effects (Fig. S6†).[15,59] Forming multiple layers on the filter paper could have also decreased the surface area and maximum electrical fields of the plasmonic NPs and their clusters prior to the treatment with the sensing molecules, which could have diminished the overall SERS enhancement and reproducibility. The light-induced temperature changes also showed a somewhat linear relationship as a function of the plasmonic NP loading and gradually reached a plateau. Thus, maintaining the cluster size of the NPs below the maximum limit plays an important role in photothermal heating and SERS applications, although the sandwich arrangement readily creates a new environment for analytes to reside near strong EM fields. Additionally, the SERS signals of the anisotropic AuNP plasmonic paper and its sandwiched layers with the AgNPs were examined as a function of time (Fig. S7†). Although nanostructured gold has shown a higher resistance to thiolate degradation, the reduction of the SERS signals for both substrates indicated the decomposition/desorption of 4-NBT at ambient conditions.[60,61] The degree of the SERS signal reductions was notably slower for the sandwiched molecules on plasmonic paper, implying the increased stability of the thiolated analyte. This observation could provide a useful clue for the surface chemistry community, which has explored diverse strategies for enhancing long-term stability of adsorbed molecules for practical applications. As a control experiment, treating unmodified glass slides with the four types of plasmonic NPs under the same preparation process resulted in very poor adsorption of the NPs which was visually observed and confirmed by their inefficient photothermal heating properties (Fig. S8a†). In addition, similar amounts of plasmonic NPs loaded onto the filter paper were dropped and dried on the glass slides. A droplet of NP solution on the glass slides took a long time to dry and visually formed a ring by random aggregation (*e.g.*, NP-dependent irregular surface coverage and coffee ring patterns to show inhomogeneous distribution), which were certainly different from the controlled assembly and packing of NPs on surface-modified glass substrates.[62–66] Given the heterogeneous loading of the NPs, the overall SERS responses were slightly weaker and notably inconsistent across the glass substrates. Specifically, the signal intensity at the edge was much higher than the center of the droplet regardless of NP types, giving notably high % RSD (Fig. S8b†), which was detectably different from the plasmonic paper substrates (Fig. S9†). This observation clearly suggests that handling paper-based materials with plasmonic NPs under our method is relatively easy to prepare highly uniform SERS substrates. In addition, considering cost-effectiveness and flexibility as well as sampling efficiency of diverse analytes, paper-based materials can be better suited to develop practical plasmonic papers for SERS substrates.

As this simple sandwich process notably improved the SERS signals by the EM effect, our system was employed in the detection of let-7f microRNA (1 μM) as a model biological molecule (Fig. 6). The spectral signature is characteristic of nucleic acid bands. The distinctive peaks at 734 cm^{-1} and 1330 cm^{-1} are attributed to adenine, whereas strong bands at 1338 cm^{-1} and 1461 cm^{-1} are characteristic of guanine.[67–69] The intense bands at 802 cm^{-1} and 1279 cm^{-1} are unique to uracil in these three sequences. Given the high molecular weight, relatively strong Raman signals were observed even with a small drop of RNA solution (50 μL) on the plasmonic paper. By simply applying the second layer of plasmonic NPs, substantial SERS enhancements clearly indicated that these macromolecules were readily retained and sandwiched near the newly-formed EM field areas. Generally, the combination of the anisotropic AuNPs and AgNPs was appreciably much higher than that of the spherical AuNPs and AuNPs. This additional experiment demonstrated the applicability of sandwich structure of plasmonic NPs in the detection of biological molecules. Our strategy

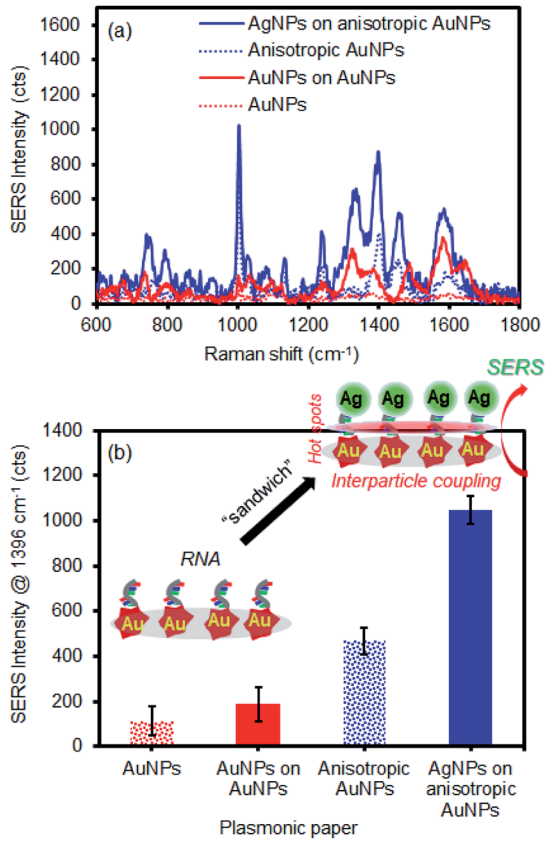

Fig. 6 Representative (a) SERS spectra of RNA on AuNP and anisotropic AuNP plasmonic paper before and after forming sandwich geometry with AuNPs and AgNPs, respectively, and (b) their average SERS intensities.

readily shows how to develop inexpensive substrates utilizing easily available plasmonic NPs and filter paper to greatly improve SERS performance for a wide range of molecules by precisely controlling the degree of hot spots and interparticle coupling.

Conclusions

Four types of plasmonic paper loaded with spherical AgNPs, AuNPs, Ag core–Au shell NPs, and anisotropic AuNPs were reliably prepared and characterized to serve as SERS substrates. The anisotropic AuNP-loaded papers exhibited a notably high SERS response due to their surface areas and structural characteristics along with a broad SPR band near the Raman excitation wavelength. Upon the addition of a second layer of plasmonic NPs to form the sandwich arrangement, the overall SERS signals were significantly enhanced by the EM effect associated with the increased probability of SPR coupling and number of hot spots. Particularly, applying the AgNPs on the anisotropic AuNP plasmonic surface resulted in the highest EM enhancement, whose calibration sensitivity and dynamic range were much higher and wider than typical AuNP–AuNP systems. Given the packing and structural properties of plasmonic NPs, the SERS-based signal enhancing patterns were greatly affected by the way the plasmonic NPs were designed and sandwiched onto a paper surface. The subsequent application of this sandwich geometry to the detection of biomolecules, such as RNA, demonstrated the possibility of developing biologically relevant signal enhancing substrates possessing important features, including high flexibility, simplicity, and cost-efficiency. Introducing a new environment for interparticle coupling and hot spots, even with readily-available plasmonic nanoparticles, still allows for highly improved SERS-based sensing capability.

Conflicts of interest

There are no conflicts to declare.

Acknowledgements

This project was supported by Award No. 2017-R2-CX-0022, awarded by the National Institute of Justice, Office of Justice Programs, U.S. Department of Justice. The opinions, findings, and conclusions or recommendations expressed in this publication are those of the authors and do not necessarily reflect those of the Department of Justice.

References

1 S.-Y. Ding, E.-M. You, Z.-Q. Tian and M. Moskovits, *Chem. Soc. Rev.*, 2017, **46**, 4042–4076.
2 H. K. Lee, Y. H. Lee, C. S. L. Koh, G. C. Phan-Quang, X. Han, C. L. Lay, H. Y. F. Sim, Y.-C. Kao, Q. An and X. Y. Ling, *Chem. Soc. Rev.*, 2019, **48**, 731–756.
3 R. J. C. Brown and M. J. T. Milton, *J. Raman Spectrosc.*, 2008, **39**, 1313–1326.
4 B. Sharma, M. F. Cardinal, S. L. Kleinman, N. G. Greeneltch, R. R. Frontiera, M. G. Blaber, G. C. Schatz and R. P. Van Duyne, *MRS Bull.*, 2013, **38**, 615–624.
5 D. P. Fromm, A. Sundaramurthy, A. Kinkhabwala, P. J. Schuck, G. S. Kino and W. E. Moerner, *J. Chem. Phys.*, 2006, **124**, 061101.
6 E. J. Zeman and G. C. Schatz, *J. Phys. Chem.*, 1987, **91**, 634–643.
7 D.-W. Li, W.-L. Zhai, Y.-T. Li and Y.-T. Long, *Microchim. Acta*, 2014, **181**, 23–43.
8 H. Dies, R. Nosrati, J. Raveendran, C. Escorbedo and A. Docoslis, *Colloids Surf., A*, 2018, **553**, 695–702.
9 H. Chen, T. You, L. Jiang, Y. Gao and P. Yin, *RSC Adv.*, 2017, **7**, 32743–32748.
10 V.-D. Phung, W.-S. Jung, T.-A. Nguyen, J.-H. Kim and S.-W. Lee, *Nanoscale*, 2018, **10**, 22493–22503.
11 H. Chang, E. Ko, H. Kang, M. G. Cha, Y.-S. Lee and D. H. Jeong, *RSC Adv.*, 2017, **7**, 40255–40261.
12 D. Cialla-May, X.-S. Zheng, K. Weber and J. Popp, *Chem. Soc. Rev.*, 2017, **46**, 3945–3961.
13 W.-L.-J. Hasi, S. Lin, X. Lin, X.-T. Lou, F. Yang, D.-Y. Lin and Z.-W. Lu, *Anal. Methods*, 2014, **6**, 9547–9553.
14 C. H. Lee, M. E. Hankus, L. Tian, P. M. Pellegrino and S. Singamaneni, *Anal. Chem.*, 2011, **83**, 8953–8958.

15 M. Lee, K. Oh, H.-K. Choi, S. G. Lee, H. J. Youn, H. L. Lee and D. H. Jeong, *ACS Sens.*, 2018, **3**, 151–159.
16 Y. H. Ngo, D. Li, G. P. Simon and G. Garnier, *Langmuir*, 2012, **28**, 8782–8790.
17 G. Weng, Y. Yang, J. Zhao, J. Zhu, J. Li and J. Zhao, *Solid State Commun.*, 2018, **272**, 67–73.
18 M. Wu, P. Li, Q. Zhu, M. Wu, H. Li and F. Lu, *Spectrochim. Acta, Part A*, 2018, **196**, 110–116.
19 G. Zheng, L. Polavarapu, L. M. Liz-Marzan, I. Pastoriza-Santos and J. Perez-Juste, *Chem. Commun.*, 2015, **51**, 4572–4575.
20 S. M. Restaino and I. M. White, *Anal. Chim. Acta*, 2018, **1060**, 17–29.
21 L. Zhang, X. Li, L. Ong, R. F. Tabor, B. A. Bowen, A. I. Fernando, A. Nilghaz, G. Garnier, S. L. Gras, X. Wang and W. Shen, *Colloids Surf., A*, 2015, **468**, 309–314.
22 J. K. Yoon, K. Kim and K. S. Shin, *J. Phys. Chem. C*, 2009, **113**, 1769–1774.
23 J. Turkevich, P. C. Stevenson and J. Hilier, *Discuss. Faraday Soc.*, 1951, **11**, 55–75.
24 M. Wuithschick, A. Birnbaum, S. Witte, M. Sztucki, U. Vainio, N. Pinna, K. Rademann, F. Emmerling, R. Kraehnert and J. Polte, *ACS Nano*, 2015, **9**, 7052–7071.
25 X. Dong, X. Ji, H. Wu, L. Zhao, J. Li and W. Yang, *J. Phys. Chem. C*, 2009, **113**, 6573–6576.
26 K. G. Stamplecoskie, J. C. Scaiano, V. S. Tiwari and H. Anis, *J. Phys. Chem. C*, 2011, **115**, 1403–1409.
27 B. W. Boote, H. Byun and J.-H. Kim, *Gold Bull.*, 2013, **46**, 185–193.
28 B. W. Boote, R. A. A. Ferreira, W. Jang, H. Byun and J.-H. Kim, *Nanotechnology*, 2015, **26**, 345701.
29 J.-H. Kim, K. M. Twaddle, L. M. Cermak, W. Jang, J. Yun and H. Byun, *Colloids Surf., A*, 2016, **498**, 20–29.
30 Y. H. Ngo, D. Li, G. P. Simon and G. Garnier, *Colloids Surf., A*, 2013, **420**, 46–52.
31 B. Li, W. Zhang, L. Chen and B. Lin, *Electrophoresis*, 2013, **34**, 2162–2168.
32 W. W. Yu and I. M. White, *Anal. Chem.*, 2010, **82**, 9626–9630.
33 J.-H. Kim, K. M. Twaddle, J. Hu and H. Byun, *ACS Appl. Mater. Interfaces*, 2014, **6**, 11514–11522.
34 A. O. Govorov and H. H. Richardson, *Nano Today*, 2007, **2**, 30–38.
35 H. H. Richardson, M. T. Carlson, P. J. Tandler, P. Hernandez and A. O. Govorov, *Nano Lett.*, 2009, **9**, 1139–1146.
36 A. M. Funston, T. J. Davis, C. Novo and P. Mulvaney, *Philos. Trans. R. Soc., A*, 2011, **369**, 3472–3482.
37 O. Neumann, A. S. Urban, J. Day, S. Lal, P. Nordlander and N. J. Halas, *ACS Nano*, 2012, **7**, 42–49.
38 Z.-C. Zeng, H. Wang, P. Johns, G. V. Hartland and Z. D. Schultz, *J. Phys. Chem. C*, 2017, **121**, 11623–11631.
39 R. Aggarwal, L. W. Farrar and S. K. Saikin, *J. Phys. Chem. C*, 2012, **116**, 16656–16659.
40 R. G. J. Strens and B. J. Wood, *Mineral. Mag.*, 1979, **43**, 347–354.
41 T. Horibe, K. Ishii, D. Fukutomi and K. Awazu, *Laser Ther.*, 2015, **24**, 303–310.
42 D. Bartkowiak, V. Merk, V. Reiter-Scherer, U. Gernert, J. P. Rabe, J. Kneipp and E. Kemnitz, *RSC Adv.*, 2016, **6**, 71557–71566.
43 S. Zhu, T. P. Chen, Z. H. Cen, E. S. M. Goh, S. F. Yu, Y. C. Liu and Y. Liu, *Opt. Express*, 2010, **18**, 21926–21931.
44 A. P. Budnyk, A. Damin, G. Agostini and A. Zecchina, *J. Phys. Chem. C*, 2010, **114**, 3857–3862.
45 A. Wei, B. Kim, B. Sadtler and S. L. Tripp, *ChemPhysChem*, 2001, **2**, 743–745.
46 L. Litti and M. Meneghetti, *Phys. Chem. Chem. Phys.*, 2019, **21**, 15515–15522.
47 M. Iatalese, M. L. Coluccio, V. Onesto, F. Amabo, E. D. Fabrizio and F. Gentile, *Nanoscale Adv.*, 2019, **1**, 228–240.
48 G. Zito, G. Rusciano, A. Vecchione, G. Pesce, R. D. Girolamo, A. Malafronte and A. Sasso, *Sci. Rep.*, 2016, **6**, 31113.
49 G. Wang, H.-Y. Park and R. J. Lipert, *Anal. Chem.*, 2009, **81**, 9643–9650.
50 K. Kim, J.-Y. Choi and K. S. Shin, *J. Phys. Chem. C*, 2015, **119**, 5187–5194.
51 K. Kim, J.-Y. Choi and K. S. Shin, *J. Phys. Chem. C*, 2014, **118**, 11397–11403.
52 Q. Cui, A. Yashchenok, L. Zhang, L. Li, A. Masic, G. Wienskol, H. Möhwald and M. Bargheer, *ACS Appl. Mater. Interfaces*, 2014, **6**, 1999–2002.
53 D. Paramelle, A. Sadovoy, S. Gorelik, P. Free, J. Hobley and D. G. Fernig, *Analyst*, 2014, **139**, 4855–4861.
54 W. Haiss, N. T. K. Thanh, J. Aveyard and D. G. Fernig, *Anal. Chem.*, 2007, **79**, 4215–4221.
55 L. G. Schulz, *J. Opt. Soc. Am.*, 1954, **44**, 357–362.
56 W. W. Yu and I. M. White, *Analyst*, 2012, **137**, 1168–1173.
57 B. Liu, H. Ni, D. Zhang, D. Wang, D. Fu, H. Chen, Z. Gu and X. Zhao, *ACS Sens.*, 2017, **2**, 1035–1043.
58 S. Sergiienko, K. Moor, K. Gudun, Z. Yelemessova and R. Bukasov, *Phys. Chem. Chem. Phys.*, 2017, **19**, 4478–4487.
59 Z. Zhu, T. Zhu and Z. Liu, *Nanotechnology*, 2004, **15**, 357–364.
60 E. Cortes, A. A. Rubert, G. Benitez, P. Carro, M. E. Vela and R. C. Salvarezza, *Langmuir*, 2009, **25**, 5661–5666.
61 Y.-S. Shon and T. R. Lee, *J. Phys. Chem. B*, 2000, **104**, 8192–8200.
62 J. Jiang, S. Wang, H. Wu, J. Zhang, H. Li, J. Jia, X. Wang and J. Liao, *RSC Adv.*, 2015, **5**, 105820–105824.
63 Y. Bu and S.-W. Lee, *Microchim. Acta*, 2015, **182**, 1313–1321.
64 M. O. Stetsenko, S. P. Rudenko, L. S. Maksimenko, B. K. Serdega, O. Pluchery and S. V. Snegir, *Nanoscale Res. Lett.*, 2017, **12**, 348.
65 X. Li, J. Zhu and B. Wei, *Chem. Soc. Rev.*, 2016, **45**, 3145–3187.
66 M. Jahn, S. Patze, I. J. Hidi, R. Knipper, A. I. Radu, A. Muhlig, S. Yuksel, V. Peksa, K. Weber, T. Mayerhofer, D. Cialla-May and J. Popp, *Analyst*, 2016, **141**, 756–793.
67 S. Yüksel, L. Schwenkbier, S. Pollok, K. Weber, D. Cialla-May and J. Popp, *Analyst*, 2015, **140**, 7254–7262.
68 F. Madzharova, Z. Heiner, M. Gühlke and J. Kneipp, *J. Phys. Chem. C*, 2016, **120**, 15415–15423.
69 R. Treffer, X. Lin, E. Bailo, T. Deckert-Gaudig and V. Deckert, *Beilstein J. Nanotechnol.*, 2011, **2**, 628–637.